PHYSICS

Rotational Doppler cooling and heating

Deng Pan[1]*, Hongxing Xu[2], F. Javier García de Abajo[1,3]*

Doppler cooling is a widely used technique to laser cool atoms, molecules, and nanoparticles by exploiting the Doppler shift associated with translational motion. The rotational Doppler effect arising from rotational coordinate transformation should similarly enable optical manipulation of the rotational motion of nanosystems. Here, we show that rotational Doppler cooling and heating (RDC and RDH) effects embody rich and unexplored physics, including an unexpected strong dependence on particle morphology. For geometrically constrained particles, cooling and heating are observed at red- or blue-detuned laser frequencies relative to particle resonances. In contrast, for nanosystems that can be modeled as solid particles, RDH appears close to resonant illumination, while detuned frequencies produce cooling of rotation. We further predict that RDH can lead to optomechanical spontaneous chiral symmetry breaking, where an achiral particle under linearly polarized illumination starts spontaneously rotating. Our results open up new exciting possibilities to control the rotational motion of nanosystems.

INTRODUCTION

The advent of lasers gave birth to various techniques for trapping and manipulating atoms, small particles, and macroscopic objects using optical forces (*1*–*5*). An important class of optical manipulation methods, such as Doppler cooling, relies on control over the dynamics of a target by exploiting the dependence of optical pressure on its velocity. As a result of the Doppler shift in the laser frequency associated with translational motion, changes in the target velocity lead to increases or reductions in the optical pressure, depending on the frequency detuning of the laser relative to the intrinsic resonances of the target. In consequence, in a particle subject to illumination by two coherent and monochromatic counter-propagating light beams, red- and blue-detuned laser frequencies can decelerate and accelerate the particle motion, respectively, thus cooling and heating the translational temperature of an ensemble of particles. The theoretical description of Doppler cooling and heating is simply a textbook result derived from classical theory. In experiments, Doppler cooling was first achieved for atoms (*6*, *7*) and recently for molecules (*8*–*12*), and it was also generalized to cool the mechanical motion of a macroscopic cavity (*13*, *14*). Compared with cooling, laser heating is less explored, although it can give rise to exciting effects such as mechanical instabilities of illuminated optical cavities (*14*).

Optical forces can also affect the rotational motion of nanosystems with rotational degrees of freedom, such as molecules (*15*–*19*) and nanoparticles (*20*–*25*). More precisely, circularly polarized light with intrinsic angular momentum can exert a torque on the particles, which is the analog of optical pressure resulting from linear momentum transfer. Compared with the optical manipulation of translational motion reviewed above, it is striking to see that the very fundamental question regarding how rotational motion affects the torque exerted by light remains unanswered. Similar to the translational counterpart, such an important piece of knowledge can be used to generalize the physics of Doppler cooling and heating to the rotational degrees of freedom. We note that, in contrast to the relatively simple instances of translationally moving inertial frames, and although rotational cooling has been achieved using specific molecules (*26*–*28*) and molecular ions (*29*–*31*), a quantum-mechanical theoretical explanation of rotational cooling involves a complex geometry-dependent coupling between optical excitations, radiation, internal rotations, and vibrational states in noninertial rotating frames (*32*–*34*); understandably, the general physics underlying rotational cooling is not yet well understood. It is thus crucial to develop a compact classical model to unveil the general physics underlying the rotational cooling effect without resorting to the internal rotational and vibrational quantum states, similar to the theoretical description of its translational counterpart. For a molecular ensemble (*15*–*19*) that is not tightly confined close to the rotational quantum ground state, the statistical average of the rotation dynamics can be approximately characterized by a continuous rotation velocity (*18*), using the quantum-classical correspondence. Such a classical model is rigorous and illuminating for studying novel optical manipulations of nano- or microparticles in the rapidly evolving field of nanophotonics (*21*–*25*, *35*–*38*).

Here, we generalize the theory of Doppler cooling and heating, usually discussed for translational motion as schematically illustrated in Fig. 1 (A and B), to deal with rotational degrees of freedom (see Fig. 1C), namely, rotational Doppler cooling and heating (RDC and RDH). We present a theory that is valid for both small particles and molecules rotating with classical velocities, which allows us to predict a marked dependence of rotational laser cooling and heating on the geometry of those particles or molecules. Specifically, for nanosystems that can be modeled as round solid particles, RDC and RDH appear in different frequency regimes compared with its translational Doppler counterpart. More notably, because of RDH, an achiral particle under linearly polarized illumination starts rotating spontaneously, manifesting a spontaneous chiral symmetry breaking (SCSB) effect. We also explore the dynamics of particles under linearly polarized illumination and find a series of stable and metastable configurations in which the particles maintain steady rotation. Our results are of fundamental importance for understanding the optical properties of rotating nanosystems, paving the way for the development of new techniques to optically manipulate rotations of nanosystems.

[1]ICFO-Institut de Ciencies Fotoniques, The Barcelona Institute of Science and Technology, 08860 Castelldefels, Barcelona, Spain. [2]School of Physics and Technology, Wuhan University, Wuhan 430072, China. [3]ICREA-Institució Catalana de Recerca i Estudis Avançats, Passeig Lluís Companys 23, 08010 Barcelona, Spain.
*Corresponding author. Email: deng.pan@icfo.eu (D.P.); javier.garciadeabajo@nanophotonics.es (F.J.G.d.A.)

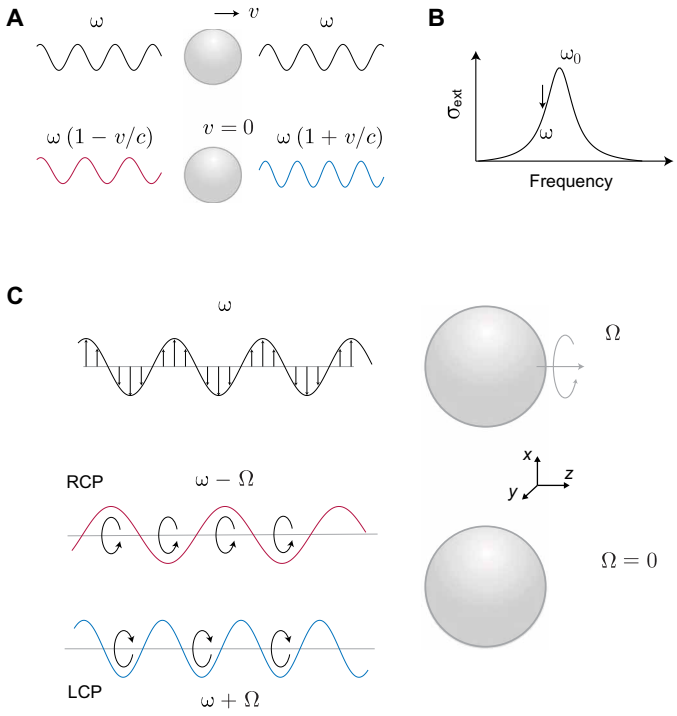

Fig. 1. Comparison between translational and rotational Doppler cooling and heating. (**A** and **B**) Illustration of translational Doppler cooling. In the laboratory frame [(A), top], a particle is moving with velocity *v* in the presence of two counter-propagating light waves (wavy curves) of frequency ω. In the frame moving with the particle [(A), bottom], the extinction cross section (σ_{ext}) of these two waves [see (B)] is affected by Doppler shifts to $\omega(1 \pm v/c)$, leading to an optical force that pushes the particle to the left, thus causing particle deceleration in the laboratory frame. (**C**) We consider a particle rotating with angular velocity Ω and illuminated by linearly polarized light of frequency ω (top). The incident light can be decomposed into right circularly polarized (RCP) and left circularly polarized (LCP) components, which are Doppler-shifted to $\omega \mp \Omega$ in the frame rotating with the particle (bottom). Black circular arrows denote the directions of the electric field rotation on the plane perpendicular to the wave vector.

RESULTS

Comparing translational and rotational scenarios

In Fig. 1A, we show a particle moving with velocity **v** and illuminated by two counter-propagating light waves of equal intensity and frequency ω (Fig. 1A, top). In the frame moving with the particle (Fig. 1A, bottom), the two light waves propagating parallel or antiparallel with **v** are red- or blue-Doppler–shifted, respectively, to $\omega(1 \pm v/c)$. Assuming a red-detuned laser frequency ω relative to a dominant intrinsic particle resonance ω_0 (Fig. 1B), compared with the red-shifted light wave, the blue-shifted antiparallel wave is closer to ω_0 and thus undergoes stronger scattering, resulting in deceleration and cooling of the particle. Similarly, heating can be achieved through blue-detuned illumination.

To generalize this scheme to rotational motion, we consider a particle trapped by a linearly polarized laser beam (Fig. 1C, top). Right and left circularly polarized (RCP and LCP) components of the incident light have then equal intensity, thus resembling the two counter-propagating waves in Fig. 1A. Then, they experience different rotational Doppler shifts to $\omega_{\mp} = \omega \mp \Omega$ (hereafter, upper and lower signs denote quantities for RCP and LCP, respectively), when transforming the system to the frame rotating with the particle (Fig. 1C, bottom), namely, a rotational Doppler effect (*15*, *39*). Similar to translational dynamics, the direction of the torque acting on the particle is then determined by the relative magnitude of the torque exerted by RCP and LCP components. One might naïvely conclude that RDC and RDH should also appear at red- and blue-detuned ω. However, as we show below, this conclusion is only valid for particles having certain geometries. Rotational transformations are noninertial, so that the optical response of the rotating particle is more complicated and thus displays richer physics. The translational trapping of particles at the antinodes of standing waves due to gradient forces cannot be extrapolated to the rotational scenario, which, as we show below, can lead to instabilities of the particle at rest ($\Omega = 0$) for laser frequencies in the heating regime.

Circular polarizabilities of rotating nanosystems

A detailed analysis of the torque exerted by linearly polarized light on rotating small particles or molecules with different geometries requires the knowledge of their optical polarizabilities. Quantum theoretical treatments of this problem commonly assume a rigid body to discuss rotation dynamics (*33*). However, the coupling between optical excitations and vibrations in molecules cannot be neglected, and importantly, this coupling has a strong dependence on geometry (*34*), which further complicates a general quantum description. Besides, a naïve application of first-order quantum perturbation theory fails to comply with the optical theorem (*40*) and therefore neglects radiative corrections that are relevant to the optical torque. To avoid this complication, here we adopt a classical model that effectively captures all relevant physical processes and retains a tutorial character to explain the dependence of RDC and RDH on particle geometry. Our model describes the dipolar optical mode of the particle as a harmonically oscillating effective charge (mass *m*, charge *Q*) driven by the electric field of light. Such classical description is capable of adequately addressing transition dipole moments, such as those of molecules, as well as resonant modes in particles. Reassuringly, this model satisfies the optical theorem (see Supplementary text) and, therefore, it correctly accounts for scattering processes. In terms of its radial position vector **r**, the classical equation of motion of the effective charge becomes

$$\ddot{\mathbf{r}} = -\omega_0^2 r\hat{r} - \gamma(\dot{\mathbf{r}} - \Omega r\hat{\varphi}) + \tau\dddot{\mathbf{r}} + \frac{Q}{m}\mathbf{E} + \frac{\mathbf{F}^{\text{react}}}{m} \quad (1)$$

where ω_0 is an intrinsic oscillator resonance frequency, we incorporate an internal dissipation force $\mathbf{F}^{\text{dis}} = -\gamma m(\dot{\mathbf{r}} - \Omega r\hat{\varphi})$ proportional to a phenomenological damping rate γ times the center-of-mass velocity, the Abraham-Lorentz force $m\tau\dddot{\mathbf{r}}$ with $\tau = 2Q^2/3mc^3$ introduces corrections due to radiation reaction, and $\mathbf{F}^{\text{react}}$ is the force imposed by the boundary defined by the particle geometry. The radial component of $\mathbf{F}^{\text{dis}}$ describes the coupling to vibrational phonons, while $\mathbf{F}^{\text{react}}$ and the azimuthal components of $\mathbf{F}^{\text{dis}}$ account for the coupling between electron motion and particle rotations.

In a thin nanorod (Fig. 2A), the oscillating dipole **p** produced by the bounded charges is oriented along the rod axis, which rotates with the particle. Likewise, in a nanocross (Fig. 2B), two dipoles (one per branch) are induced, also rotating with the particle. In contrast, for isotropic nanoparticles containing freely moving electrons, such as the nanodisk shown in Fig. 2C, we need to consider the coupling between the two orthogonal charge oscillators through the Coriolis force. At this point, it is useful to consider the electric

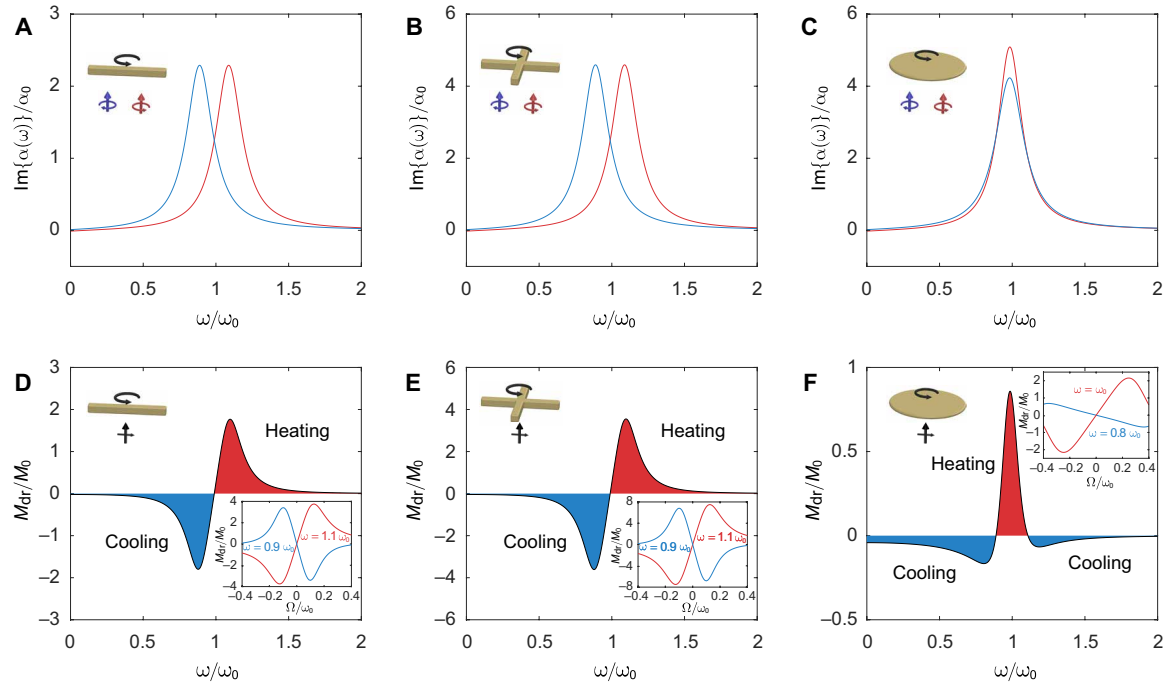

Fig. 2. Optical torque acting on rotating particles. (**A** to **C**) Optical response of rotating particles of different geometries, namely, nanorod (A), nanocross (B), and nanodisk (C), to RCP (red) and LCP (blue) incident light. We plot the imaginary part of the polarizability, which is related to the extinction cross section according to $\sigma_{ext} = (4\pi\omega/c)\,\mathrm{Im}\{\alpha\}$. A solid particle such as the nanodisk (C) exhibits different circular dichroism relative to particles with confined electron motion, such as the nanorod (A) and nanocross (B). (**D** to **F**) Time-averaged torque M_{dr} acting on the rotating particles considered in (A) to (C) under linearly polarized illumination. Insets: M_{dr} versus particle rotating frequency Ω for two typical light frequencies in the cooling and heating regimes. In all cases, damping rates are assumed to be $\gamma = 0.2\omega_0$ and $\tau^{-1} = 0.02\omega_0$. Apart from the insets, particles are rotating with angular velocity $\Omega = 0.1\omega_0$. All frequencies are normalized to the particle resonance frequency ω_0, the polarizability is normalized to $\alpha_0 = Q^2/m\omega_0^2$, and the torque is normalized to $M_0 = \alpha_0 |E_\pm|^2/2$. We assume a large resonance linewidth for illustration.

field $\mathbf{E}_\pm = (\hat{x} \pm i\hat{y})E_\pm e^{-i\omega t}/\sqrt{2}$ of RCP (+) and LCP (−) light and relate the induced elastic dipole moment $\mathbf{p}_\pm^\omega = \alpha_\pm \mathbf{E}_\pm$ (oscillating at frequency ω in the laboratory frame) to the circular polarizability of the particle $\alpha_\pm$. In this work, the particle rotation axis is assumed to be along the *z* direction and only the electric field component in the *x*-*y* plane is relevant to the physics, so we define the chirality of the light field (i.e., LCP and RCP) according to the rotation direction of $\boldsymbol{E}_{pm}$ (see Fig. 1C), regardless of the direction of the photon wave vector. We note that $\mathbf{p}_\pm^\omega$ is formed by two orthogonal degenerate components. Applying Eq. 1 to these three representative types of particles (see Methods, Supplementary text, and fig. S1), we find

$$\alpha_\pm(\omega) = Q^2/mA \tag{2}$$

with

$$A_{rod} = 2[\omega_0^2 - \Omega^2 - \omega_\mp^2 - i\omega_\mp(\gamma + \tau\omega_\mp^2 + 3\tau\Omega^2)]$$
$$A_{cross} = \omega_0^2 - \Omega^2 - \omega_\mp^2 - i(\gamma\omega_\mp + \tau\omega^3)$$
$$A_{disk} = \omega_0^2 - \Omega^2 - \omega^2 - i(\gamma\omega_\mp + \tau\omega^3)$$

where *Q* denotes the total effective charge in the nanorod, while the cross and disk have a charge of *Q* oscillating along each of the two orthogonal directions. Such theory can be rigorous in classical scenarios, such as nanoparticles and molecules consisting of larger numbers of atoms, with rotation energy not tightly confined close to the rotational ground state.

This classical model treats the rotation of particles as a continuum of states characterized by a rotation frequency Ω, which we remark can always be considered as a rigorous approach for nanoparticles and molecules consisting of a large number of atoms. For an ensemble of small molecules containing only a few atoms (e.g., diatomic molecules) and rotating with high angular velocity, according to the quantum-classical correspondence guaranteed by the Ehrenfest theorem, the statistical average of the rotational dynamics can then also be characterized by the rotation frequency Ω, so the molecular dynamics is adequately described through our classical model. For example, the rotational Raman scattering observed in molecules (*15*, *39*) with a high rotation frequency is captured by our model without resorting to quantized rotational modes (see results below). When small molecules are gradually cooled down to extremely low temperatures and the rotation energy is lowered near the quantum rotational ground state, the quantization of the rotational states becomes increasingly more important. However, since the general physical description should be consistent in both classical and quantum scenarios, as already demonstrated in the translational Doppler cooling, our model and the results obtained from it below still offer qualitative understanding to estimate the behavior of electron-phonon/rotations interaction in the quantum limit. As reviewed in Introduction, the complicated morphology-dependent coupling between electrons and phonon/rotations in molecules conceals the essential physics underlying rotational cooling. As we show below, our simple model is capable of intuitively capturing the geometry dependence of the coupling between material electrons and rotational modes.

Optical torque exerted by linearly polarized light

The polarizabilities given by Eq. 2 can fully describe the optical response of small rotating particles and the optical torque produced under external illumination. According to the optical theorem, the extinction cross sections of these particles are given by $\sigma_{ext}^{\pm} = 4\pi k \mathrm{Im}\{\alpha_{\pm}\}$, where $k = \omega/c$. However, elastic scattering processes, as described by the cross section $\sigma_{\omega}^{\pm} = 8\pi k^4 |\alpha_{\pm}|^2/3$, maintain the angular momentum of light and thus do not lead to a torque on the particle. In contrast, each absorbed circularly polarized photon directly transfers angular momentum $\hbar$ to the particle, so we are interested in the absorption cross section $\sigma_{abs}^{\pm} = \sigma_{ext}^{\pm} - \sigma_{\omega}^{\pm} - \sigma_{\omega\mp2\Omega}^{\pm}$. Here, $\sigma_{\omega\mp2\Omega}^{\pm}$ is the cross section of inelastic scattering at output frequency $\omega \mp 2\Omega$ [the so-called rotational Doppler scattering or rotational Raman scattering (*15*, *39*); see Supplementary text], which is only present in rotating anisotropic particles and comes accompanied by an exchange of angular momentum $2\hbar$ and energy $2\hbar\Omega$ for each scattered photon. For the nanorod, we find $\sigma_{\omega\mp2\Omega}^{\pm} = 8\pi(\omega \mp 2\Omega)^4 |\alpha_{\pm}|^2/3c^4$, while this cross section vanishes for the cross and the disk. Last, the total torque exerted on the particle by RCP and LCP components reduces to

$$M_{\pm} = \pm(2\eta\sigma_{\omega\mp2\Omega}^{\pm} + \sigma_{abs}^{\pm})\, I/\omega \tag{3}$$

where $I = c|E_{\pm}|^2/8\pi$ is the incident light intensity, and $\eta = \omega_{\mp}/(\omega \mp 2\Omega)$ accounts for the energy shifts of inelastically scattered photons.

Figure 2 (A to C) shows the imaginary part of the circular polarizabilities $\mathrm{Im}\{\alpha_{\pm}\}$ for the three types of rotating particles described by Eq. 2, whose internal losses dominate over radiative losses ($\gamma \gg \tau^{-1}$). We observe a strong circular dichroism (CD) in the rotating thin nanorod and nanocross, characterized by a splitting of 2Ω in the resonance peaks. Similar dichroism can also be observed in particles without internal dissipation (i.e., for $\gamma = 0$, see fig. S2). In contrast, the polarizability of the rotating disk with freely moving electrons inside it does not exhibit any resonance splitting. However, the factor A_{disk} in Eq. 2 predicts a difference in the decay rate for different circular polarizations, which leads to a weak CD, manifested by the discrepancy in the linewidth and magnitude of the resonance peaks in Fig. 2C.

Provided with the CD response of these rotating particles, we can readily conclude that linearly polarized illumination should exert optical torques on the particles because this type of light can be decomposed into RCP and LCP components with equal amplitudes, which contribute with opposite and imbalanced torques. Figure 2 (D to F) shows rigorous results for the total optical torque experienced by the particles described in Fig. 2 (A to C) under linearly polarized light, calculated from Eq. 3 according to $M_{dr} = M_+ + M_-$. For particles with $\gamma \gg \tau^{-1}$, such as those considered in Fig. 2, Eq. 3 can be approximated as $M_{\pm} \approx 2\,\mathrm{Im}\{\alpha_{\pm}\}|E_{\pm}|^2$, so that the torques in Fig. 2 (D to F) are proportional to $\mathrm{Im}\{\alpha_{\pm}\}$, as shown in Fig. 2 (A to C). For example, for rotating nanorods and nanocrosses under red-detuned laser illumination ($\omega < \omega_0$; Fig. 2, A and B), absorption of the LCP component should be strong compared with that of the RCP component ($\mathrm{Im}\{\alpha_-\} > \mathrm{Im}\{\alpha_+\}$), so that the total torque exerted by linearly polarized light should decelerate the particle rotation, leading to an RDC effect (blue shaded area in Fig. 2, D and E; see Supplementary text for discussions on the RDC limit). Similarly, rotational acceleration (red shaded area in Fig. 2, D and E) is observed for blue-detuned illumination ($\omega > \omega_0$). The RDC and RDH effects are also confirmed by the dependence of M_{dr} on Ω (insets in Fig. 2, D and E), which is similar to the velocity dependence of optical pressure in optical molasses. The conditions for RDC and RDH in rotating nanorods and nanodisks are also similar to those for their translational counterparts. This similarity originates in the fact that the polarizability observed in the rotating frame is equal to that of the motionless particle, $\alpha_+(\omega_+) = \alpha_-(\omega_-) \approx \alpha(\omega, \Omega = 0)$, so that the discussions for translational cooling based on Fig. 1B are equivalently applied to rotating particles with these types of geometries. However, for a rotating solid particle, such as the disk shown in Fig. 2F, because of its different CD shown in Fig. 2C, an RDH effect is observed for a nearly resonant laser frequency ω, while RDC is found at off-resonance laser frequencies in both blue- and red-detuned regimes. We also note that the dissipationless limit ($\gamma = 0$), in which the torque acting on isotropic particles disappears according to Eq. 3, is generally unphysical because dissipation channels are generally present in molecules and nanoparticles that can quench optical excitations. Even in the limit $\gamma = 0$ (rigid molecules), RDC and RDH effects can be observed in anisotropic particles because of the torque arising in rotational Raman scattering (see Eq. 3 and fig. S2).

Rotational stability and dynamics

Besides the optical torque discussed in Fig. 2, light absorption can also increase the temperature of a particle or the vibration energy of a molecule, and the subsequent thermal emission can produce a frictional torque on the particle if it is rotating (*41*–*43*). This thermal frictional torque arises because the two circularly polarized dipoles $\mathbf{p}_{\pm}$ have different thermal populations and, therefore, there is an imbalance in the angular momentum released through thermal emission, leading to a frictional torque (see Methods)

$$M_{fr} = -c\hbar\sum_{\nu=\pm}\nu\int_0^{\infty} d\omega\, \rho^0(\omega)\, \sigma_{abs}^{\nu} N_{\nu}(\omega) \tag{4}$$

where $N_{\pm}(\omega) = n_1(\omega_{\mp}) - n_0(\omega)$ is the thermal imbalance of particle modes with vacuum, and $\rho_0(\omega) = \omega^2/3\pi^2c^3$ is the projected local density of optical states in free space. For rotating particles, when the light frequency falls into the cooling regime, both thermal friction and optical cooling lead to slowing down of rotation; consequently, provided the light frequency is in the heating regime, the driving torque M_{dr} exerted by the external illumination needs to exceed the thermal friction M_{fr} to produce acceleration.

An interesting phenomenon can be intuitively foreseen for a particle at rest under linearly polarized illumination when the light frequency is in the heating regime: If the condition $\partial_{\Omega}M_{dr} > \partial_{\Omega}M_{fr}$ is satisfied at $\Omega = 0$, a small particle rotation induced by any fluctuation can be amplified by RDH. This effect implies an instability of the particle at rest, and considering the chiral symmetry of the system Hamiltonian, such instability manifests as an SCSB process. We note that the SCSB term relates to the dynamics of a single particle, while for an ensemble, the statistical average cancels the macroscopic chirality. To further analyze the particle stability at $\Omega = 0$, we need to find the steady state of the particle temperature under light irradiation, which is reached when the power absorbed from the laser, $P_{abs} = \Sigma_{\pm} I_{\pm} \sigma_{abs}^{\pm}$, is exactly compensated by the thermal-emission power. At arbitrary Ω, the latter is given by (*42*) (see Methods)

$$P_{ems} = c\hbar\sum_{\nu=\pm}\int_0^{\infty} \omega d\omega\, \rho^0(\omega)\, \sigma_{abs}^{\nu} N_{\nu}(\omega) \tag{5}$$

The stability of the particle can be investigated by taking the following aspects into account: (i) given the environment temperature T_0, under stationary conditions, the laser intensity is uniquely determined by the particle temperature $I(T_1)$; (ii) the driving torque $\partial_\Omega M_{dr}$ is then uniquely related to T_1 through $I(T_1)$; (iii) $\partial_\Omega M_{fr}$ depends on T_0 and T_1, and its magnitude compared with $\partial_\Omega M_{dr}$ determines the stability. Following these considerations, at a given incident frequency ω, the rotational stability of the particle can be mapped into a T_0 versus T_1 plot.

In Fig. 3A, we choose the nanocross of Fig. 2B at rest ($\Omega = 0$) as an example to illustrate the stability in the (T_0, T_1) plane, and in fact, this diagram of stability also represents the nanorod in Fig. 2A (see discussion on the nanodisk in Fig. 2C and fig. S3). This plot constitutes a universal phase diagram, considering that phase transitions are featured by spontaneous symmetry breaking—in the normal phase, the motionless state is stable; when increasing the intensity of illumination I to heat the particle above the critical temperature dictated by the phase boundary in Fig. 3A (black curves), the particle starts rotating spontaneously and the system enters into an SCSB phase.

To clearly reveal the features of the SCSB phase and find the final stable configuration, we simulate the evolution of Ω and T_1 as governed by the dynamical equations of motion $\dot{\Omega} = M_{tot}/J$ and $\dot{T}_1 = (P_{abs} - P_{ems} - M_{tot}\Omega)/C$, where $M_{tot} = M_{dr} - M_{fr}$, and J and C are the moment of inertia and thermal capacity of the particle, respectively. The evolution of the system for a vacuum temperature $T_0 = 0.4\Theta_0$, where $\Theta_0 = \hbar\omega_0/k_B$, is shown in Fig. 3 (B and C), taking the laser intensities to be either $I(0.41\Theta_0)$ or $I(0.5\Theta_0)$, corresponding to points I and II in Fig. 3A, respectively. Here, we discuss the general behavior of rotational heating based on normalized quantities, so we can easily obtain absolute values for specific particles based on Fig. 3 (an example is shown in fig. S4).

For an incident frequency $\omega = 1.1\omega_0$, the two points in Fig. 3A fall into normal and SCSB phases, respectively (see boundary shown as a black solid curve in Fig. 3A). When the system is in the normal phase, as shown in Fig. 3B, regardless of the initial conditions for Ω and T_1, the system evolves toward a trivial stable equilibrium point (black dot) at $\Omega = 0$ and $T_1 = 0.41\Theta_0$, since the laser intensity used is $I(0.41\Theta_0)$. By increasing the laser intensity to $I(0.5\Theta_0)$, the equilibrium point located at $\Omega = 0$ is shifted to higher temperature at $T_1 = 0.5\Theta_0$ (gray dot). As expected, this equilibrium point becomes unstable, and the particle then starts rotating toward a random direction, which eventually reaches one of the two new stable equilibrium states (black dots, Fig. 3C). The characteristics of the normal and SCSB phases revealed by these dynamical evolutions are

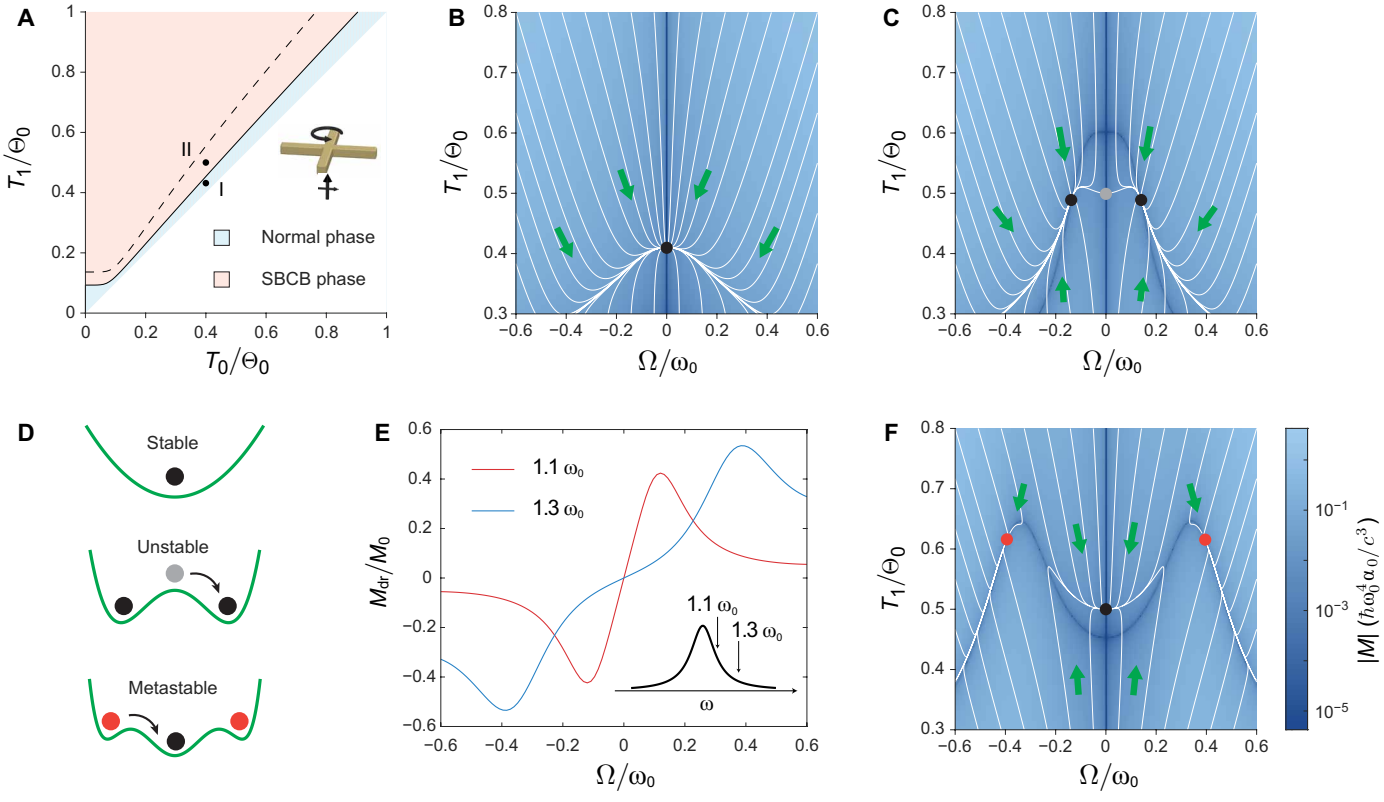

Fig. 3. Rotational dynamics of particles under linearly polarized illumination. (**A**) Stability of the nanocross considered in Fig. 2 (B and E) at rest under linearly polarized illumination of frequency $\omega = 1.1\omega_0$ (solid curve) and $1.3\omega_0$ (dashed curve), as a function of vacuum and particle temperatures T_0 and T_1 normalized to $\Theta_0 = \hbar\omega_0/k_B$. For each value of T_0, a steady particle temperature T_1 is reached at a laser intensity $I(T_1)$. The black solid and dashed curves denote phase boundaries for frequencies $\omega = 1.1\omega_0$ and $1.3\omega_0$, respectively. (**B** and **C**) Evolution of the nanocross at arbitrary initial T_1 and Ω for light frequency $\omega = 1.1\omega_0$, with vacuum temperature $T_0 = 0.4\Theta_0$ and laser intensities $I(0.41\Theta_0)$ (B) or $I(0.5\Theta_0)$ (C), which correspond to the black dots I and II in (A). (**D**) Illustration of the particle state in different phases. Top: The equilibrium state at $\Omega = 0$ is stable [black dot, also in (B)]. Middle: The equilibrium state at $\Omega = 0$ is unstable for high light intensity [gray dot, also in (C)]. Bottom: A metastable configuration (see below). (**E**) Driving torque acting on the particle rotating at different velocities Ω for light frequencies $\omega = 1.1\omega_0$ and $1.3\omega_0$. (**F**) Same as (C) for light frequency $\omega = 1.3\omega_0$. Two metastable configurations are observed, yielding the equilibrium at $\Omega = 0$ stable [point II in (A) is in the normal phase for $\omega = 1.3\omega_0$], which is intuitively illustrated in the bottom panel of (D).

intuitively illustrated in Fig. 3D (top and middle), where the black and gray dots correspond to the stable and unstable equilibrium states in Fig. 3 (B and C).

In Fig. 3A, the phase boundary for $\omega = 1.3\omega_0$ is also indicated through a dashed curve, which lies above the phase boundary for $\omega = 1.1\omega_0$. As shown in Fig. 3E, given a fixed laser intensity, the particle acquires a large optical torque from a laser at $\omega = 1.1\omega_0$ at a small rotation frequency $\Omega \approx 0$ compared to $\omega = 1.3\omega_0$, so a laser with frequency $\omega = 1.1\omega_0$ can more easily break the stability at $\Omega = 0$. Point II for $\omega = 1.3\omega_0$ lies within the normal phase, and the corresponding dynamical evolution is shown in Fig. 3F. Although the equilibrium state at $\Omega = 0$ in Fig. 3F is stable, we also observe two metastable configurations (red dots) at relatively high rotation frequency, which arise because a larger driving torque can be exerted at a far-detuned frequency $\omega = 1.3\omega_0$ for higher Ω (Fig. 3E). In the metastable state, the particle can maintain its rotation, and only a large perturbation comparable to the energy barrier surrounding the metastable region can break the stability and induce the particle to return to equilibrium at $\Omega = 0$, as illustrated in Fig. 3D (bottom). The stable and metastable states for finite rotation velocity revealed in Fig. 3 (C and F) should also be observed in a nanocross with small anisotropy, since the time-averaged torque acting on the rotating particle should then vanish. However, for $\Omega \approx 0$, such torque tends to align the long axis of the particle with the direction of linear polarization, which can increase the threshold temperature T_1 shown by the curve in Fig. 3A and, consequently, also the corresponding laser intensity.

DISCUSSION

In Figs. 2 and 3, we choose a large linewidth to illustrate the mechanisms involved in RDC and RDH. For small particles with $\gamma > \tau^{-1}$, according to $\partial_\Omega M_{\mathrm{dr}} \propto \partial_\Omega \,\mathrm{Im}\,\{\alpha(\omega)\}$ (near $\Omega = 0$), the predicted phenomena are more easily attainable in particles with sharp resonances. We also note that a high rotation frequency Ω comparable with ω_0 is adopted here also for intuitive illustrations, whereas RDC and RDH are readily observed for lower rotation frequency, as can be seen in Fig. 2 (insets in D to F). Detailed calculations also show that the predicted RDC and RDH in this work can be achieved for plasmonic nanoparticles, where all necessary conditions are feasible using currently available experimental techniques (see fig. S5).

Regarding various new materials emerging in nanophotonics, we argue that graphene particles with high electron mobility are good candidates to test the predicted phenomena, since they sustain ultranarrow plasmon resonances at long wavelength, which also help reduce thermal friction. Optomechanical SCSB should be achievable in graphene, since the electron temperature of this material (i.e., T_1) can easily reach $\sim 10^3$ K and exceed Θ_0 under external illumination. Sparse particles or molecules trapped in a high vacuum could be used to avoid gas friction and coupling between rotational and translational degrees of freedom originating in these scattering events. In experiments, concepts and techniques that are well developed in current optical cooling setups, such as Zeeman splitting and chirping of the light frequency, could be combined with the mechanism here revealed to explore actual applications. We also note that the optical response of a rotating nanoring is similar to a nanocross (*34*). Considering a ring particle with high electron mobility, with its lattice fixed in the laboratory frame and exposed to linearly polarized illumination, we expect a spontaneous electron current to arise, mimicking the mechanical rotation in our model. However, we argue that such spontaneous electron current cannot be achieved in a nanodisk according to our model dealing only with the linear response (*44*), because CD as in Fig. 2C cannot be observed in such case. Our work unveils fundamental mechanisms enabling new approaches toward optical trapping and also offers unexplored insights into the optical response of out-of-equilibrium rotating systems.

METHODS

Modeling circular polarizabilities

Our model extends a previously formulated approach (see details in Supplementary text) (*45*). To find the circular polarizability of a rotating nanosystem, we need to solve the motion of the effective charge inside the particle (position vector $\mathbf{r}_\pm$), which is governed by Eq. 1 for a circularly polarized optical electric field $\mathbf{E}_\pm = (\hat{x} \pm i\hat{y})\, E_\pm e^{-i\omega t}/\sqrt{2}$. This directly leads to an induced electric dipole moment $\mathbf{p}_\pm = Q\mathbf{r}_\pm$. In the laboratory frame, the electric dipole moment in a rotating particle of arbitrary symmetry should include in general two Fourier components, $\mathbf{p}_\pm = \mathbf{p}_\pm^{\omega} + \mathbf{p}_\pm^{\omega \mp 2\Omega}$, where $\mathbf{p}_\pm^{\omega}$ and $\mathbf{p}_\pm^{\omega \mp 2\Omega}$ are associated with frequencies ω and $\omega \mp 2\Omega$, respectively. Here, we define the circular polarizability through the elastic electric dipole relation $\mathbf{p}_\pm^{\omega} = \alpha_\pm \mathbf{E}_\pm$.

In a thin nanorod (Fig. 2A), the oscillating dipole $\mathbf{p}$ produced by the bounded charge is oriented along the rod axis, which rotates with the particle. We assume that the rod axis is fixed to x' in the Cartesian coordinate system rotating with the nanorod ($x' - y'$, see fig. S1A), so that Eq. 1 reduces to one-dimensional motion in the rotating frame. For RCP (+) and LCP (−) light, the electric field $\mathbf{E}_\pm(\omega)$ in the rotating frame is Doppler-shifted to frequency $\omega \mp \Omega$ (see Fig. 1C), which forces the charge to oscillate also at the same frequency $\omega \mp \Omega$. However, when observed in the laboratory frame, the charge oscillation in the nanorod includes Fourier components at frequencies ω and $\omega \mp 2\Omega$, which correspond to elastic and inelastic scattering processes, respectively. For an optically isotropic nanoparticle, the total dipole moment $\mathbf{p}_\pm$ is the sum of two orthogonal degenerate rotating dipole moments, $\mathbf{p}_{\pm,1}$ and $\mathbf{p}_{\pm,2}$. An example of an optically isotropic particle is formed by connecting two orthogonal nanorods at their centers with two branches fixed along x' and y' (see Fig. 2B and fig. S1B), where we assume a charge Q oscillating along each of the two orthogonal directions. Another example of an optically isotropic particle is a nanodisk (see Fig. 2C and fig. S1C), which contains freely moving electrons. In these optically isotropic particles, the superposition of the elastic dipole moments from the two orthogonal oscillations $\mathbf{p}_{\pm,1}^{\omega} + \mathbf{p}_{\pm,2}^{\omega}$ add up constructively, while the inelastic dipole moments $\mathbf{p}_{\pm,1}^{\omega \mp 2\Omega} + \mathbf{p}_{\pm,2}^{\omega \mp 2\Omega}$ cancel out. In contrast, inelastic scattering is present in optically anisotropic nanorods, which manifests as a discrepancy in the losses captured by the imaginary parts of A_{rod} and $A_{\mathrm{cross,\,disk}}$ in Eq. 2. The real parts of A_{rod} and A_{cross} are the same because the electron motions in these two types of particles are both confined to the radial directions, thus leading to similar resonance frequency shifts (see Fig. 2, A and B). However, a disk shows different resonance behavior, as shown by the real part of A_{disk} and Fig. 2C, because its internal electrons can move freely in the absence of a reaction force $\mathbf{F}^{\mathrm{react}}$ in Eq. 1.

Optical cross sections

The time-averaged powers associated with the different physical processes, described by the force terms in Eq. 1, can be easily calculated as $P = \langle \mathbf{F} \cdot \dot{\mathbf{r}} \rangle$. By inserting here the force terms of Eq. 1, including

the light field force $Q\mathbf{E}$, the Abraham-Lorentz force $m\tau\ddot{\mathbf{r}}$, the dissipation force $\mathbf{F}^{\mathrm{dis}}$, and the reaction force $\mathbf{F}^{\mathrm{react}}$ (solved according to the force balance in Eq. 1), we can find the extinction (P_{ext}), scattering (P_{sca}), dissipation (P_{dis}), and mechanical power (P_{react}) contributions to P, respectively. The extinction and scattering powers are consistent with conventional definitions for motionless particles, which describe the powers of the total input energy and the re-emission of the dipole moments. The dissipation and mechanical power are associated with the energy converted to heat and rotational energy, respectively, and these two components constitute the absorption energy that is stored in the particle, $P_{\mathrm{abs}} = P_{\mathrm{sca}} + P_{\mathrm{dis}}$. Likewise, these four force terms also allow us to find the corresponding time-averaged optical torques according to $\mathbf{M} = \langle \mathbf{r} \times \mathbf{F} \rangle$ (see details in Supplementary text). In particular, the sum of the torques exerted by $\mathbf{F}^{\mathrm{dis}}$ and $\mathbf{F}^{\mathrm{react}}$ stand for the net torque acting on the particle.

As mentioned in previous sections, the time-averaged powers and optical torques permit us to define the optical cross section as $\sigma = P/I$. From the partial powers found above, we further obtain the extinction (σ_{ext}), scattering (σ_{sca}), dissipation (σ_{dis}), and mechanical (σ_{react}) cross sections. As the absorption power P_{abs} is the sum of P_{sca} and P_{dis}, the absorption cross section corresponds to the sum $\sigma_{\mathrm{abs}} = \sigma_{\mathrm{dis}} + \sigma_{\mathrm{react}}$. Energy conservation is thus stated in terms of these cross sections as $\sigma_{\mathrm{ext}} = \sigma_{\mathrm{sca}} + \sigma_{\mathrm{abs}}$. In addition, by separating the scattering power into elastic and inelastic components, corresponding to the emission powers associated with $\mathbf{p}^{\omega}$ and $\mathbf{p}^{\omega \mp p2\Omega}$, we can define the elastic and inelastic scattering cross sections σ_{ω} and $\sigma_{\omega \mp 2\Omega}$. Now, we can recast the net optical torque acting on the particle in a compact form using these cross sections, as shown in Eq. 3.

Torque due to exchanges with the thermal field

To determine the optical torque acting on rotating particles due to thermal radiation, we consider optical absorption from the vacuum thermal field, as well as radiation emission (i.e., the reciprocal process). Vacuum photon modes can be represented by a complete set of plane waves, each of them characterized by a wave vector $\mathbf{k}$ and a polarization vector $\hat{\mathbf{e}}_i$, where $\hat{\mathbf{e}}_i$ can be chosen to run over two orthogonal linear polarizations. For the thin nanoparticles considered in Fig. 2, only the electric field components in the x-y plane perpendicular to the rotation axis (see fig. S1) are relevant to light absorption and emission. By further projecting the polarization vector onto the in-plane circular polarization unit vectors $\hat{\mathbf{u}}_{\pm} = (\hat{x} \pm \mathrm{i}\hat{y})/\sqrt{2}$, we find the effective number of photons absorbed from each incident plane wave mode to be $c\,\sigma_{\mathrm{abs}}^{\pm}\,|\,\hat{\mathbf{e}}_i \cdot \hat{\mathbf{u}}_{\pm}\,|^2/V$, where V is the quantization volume; each of these photons transfers an angular momentum $\pm\hbar$ to the particle. Now, the number of photons in each plane wave mode of frequency ω is given by $n_0(\omega)$, the Bose-Einstein distribution evaluated at the vacuum temperature T_0. By summing contributions from modes with all possible wave vectors $\mathbf{k}$ and taking into account the photon population, we find the total absorption rate of thermal photons to be

$$\Gamma_{\pm}^{\mathrm{abs}} = \frac{c}{V}\sum_{i,\mathbf{k}} \sigma_{\mathrm{abs}}^{\pm}\, n_0(\omega)\,[n_1(\omega_{\mp})+1]\;|\,\hat{\mathbf{e}}_i \cdot \hat{\mathbf{u}}_{\pm}\,|^2$$
$$= \frac{1}{3\pi^2 c^2}\int_0^{\infty} \omega^2\, \mathrm{d}\omega\, \sigma_{\mathrm{abs}}^{\pm}\, n_0(\omega)\,[n_1(\omega_{\mp})+1]$$

where we have carried out the sum over modes using the relations $V^{-1}\Sigma_{i,\mathbf{k}}|\,\hat{\mathbf{e}}_i \cdot \hat{\mathbf{u}}_{\pm}\,|^2 = (2\pi)^{-3}\int \mathrm{d}\mathbf{k}\,\Sigma_i|\,\hat{\mathbf{e}}_i \cdot \hat{\mathbf{u}}_{\pm}\,|^2 = \int \omega^2 d^{\omega}/3\pi^2 c^3$, and we have introduced a factor $n_1(\omega_{\mp}) + 1$ to represent the fact that a (bosonic) particle polarization mode of Doppler-shifted frequency $\omega_{\mp}$ has increased its population from $n_1(\omega_{\mp})$ (the Bose-Einstein distribution at the particle temperature T_1) to $n_1(\omega_{\mp}) + 1$. Similarly, the thermal photon emission rate only differs from the absorption rate in the changes incurred on the thermal distributions, with a particle mode and a photon mode decreasing and increasing their populations by 1, respectively. We find

$$\Gamma_{\pm}^{\mathrm{emi}} = \frac{1}{3\pi^2 c^2}\int_0^{\infty} \omega^2\, \mathrm{d}\omega\, \sigma_{\mathrm{abs}}^{\pm}\,[n_0(\omega)+1]\,n_1(\omega_{\mp}).$$

The absorption and emission of each photon are accompanied by a transfer of angular momentum $\pm\hbar$, so the net torque on the rotating particle is

$$M_{\mathrm{fri}} = \sum_{\pm}(\pm\hbar)\,(\Gamma_{\pm}^{\mathrm{abs}} - \Gamma_{\pm}^{\mathrm{emi}})$$

which readily leads to Eq. 4. Likewise, the absorption and emission of each photon are accompanied by an energy exchange $\hbar\omega$, so we find that the net emission power from a rotating particle reduces to

$$P_{\mathrm{emi}} = \sum_{\pm}\hbar\omega(\Gamma_{\pm}^{\mathrm{emi}} - \Gamma_{\pm}^{\mathrm{abs}})$$

which directly leads to Eq. 5. Incidentally, there is no contribution to the net power that does not experience a rotational Doppler shift because the particle is assumed to be thin along the rotation direction and, therefore, the emission associated with polarization along that axis can be neglected.

SUPPLEMENTARY MATERIALS

Supplementary material for this article is available at http://advances.sciencemag.org/cgi/content/full/7/2/eabd6705/DC1

REFERENCES AND NOTES

1. A. Ashkin, Acceleration and trapping of particles by radiation pressure. *Phys. Rev. Lett.* **24**, 156–159 (1970).
2. A. Ashkin, J. M. Dziedzic, Optical levitation by radiation pressure. *Appl. Phys. Lett.* **19**, 283–285 (1971).
3. A. Ashkin, J. M. Dziedzic, J. E. Bjorkholm, S. Chu, Observation of a single-beam gradient force optical trap for dielectric particles. *Opt. Lett.* **11**, 288–290 (1986).
4. P. F. Cohadon, A. Heidmann, M. Pinard, Cooling of a mirror by radiation pressure. *Phys. Rev. Lett.* **83**, 3174 (1999).
5. O. Arcizet, P.-F. Cohadon, T. Briant, M. Pinard, A. Heidmann, J.-M. Mackowski, C. Michel, L. Pinard, O. Français, L. Rousseau, High-sensitivity optical monitoring of a micromechanical resonator with a quantum-limited optomechanical sensor. *Phys. Rev. Lett.* **97**, 133601 (2006).
6. D. J. Wineland, R. E. Drullinger, F. L. Walls, Radiation-pressure cooling of bound resonant absorbers. *Phys. Rev. Lett.* **40**, 1639 (1978).
7. S. Chu, L. Hollberg, J. E. Bjorkholm, A. Cable, A. Ashkin, Three-dimensional viscous confinement and cooling of atoms by resonance radiation pressure. *Phys. Rev. Lett.* **55**, 48 (1985).
8. E. S. Shuman, J. F. Barry, D. DeMille, Laser cooling of a diatomic molecule. *Nature* **467**, 820 (2010).
9. M. T. Hummon, M. Yeo, B. K. Stuhl, A. L. Collopy, Y. Xia, J. Ye, 2D magneto-optical trapping of diatomic molecules. *Phys. Rev. Lett.* **110**, 143001 (2013).
10. J. F. Barry, D. J. McCarron, E. B. Norrgard, M. H. Steinecker, D. DeMille, Magneto-optical trapping of a diatomic molecule. *Nature* **512**, 286 (2014).
11. S. Truppe, H. J. Williams, M. Hambach, L. Caldwell, N. J. Fitch, E. A. Hinds, B. E. Sauer, M. R. Tarbutt, Molecules cooled below the Doppler limit. *Nat. Phys.* **13**, 1173–1176 (2017).
12. L. Anderegg, B. L. Augenbraun, Y. Bao, S. Burchesky, L. W. Cheuk, W. Ketterle, J. M. Doyle, Laser cooling of optically trapped molecules. *Nat. Phys.* **14**, 890–893 (2018).
13. J. Chan, T. P. M. Alegre, A. H. Safavi-Naeini, J. T. Hill, A. Krause, S. Gröblacher, M. Aspelmeyer, O. Painter, Laser cooling of a nanomechanical oscillator into its quantum ground state. *Nature* **478**, 89–92 (2011).

14. O. Arcizet, P. F. Cohadon, T. Briant, M. Pinard, A. Heidmann, Radiation-pressure cooling and optomechanical instability of a micromirror. *Nature* **444**, 71–74 (2006).
15. O. Korech, U. Steinitz, R. J. Gordon, I. S. Averbukh, Y. Prior, Observing molecular spinning via the rotational Doppler effect. *Nat. Photonics* **7**, 711–714 (2013).
16. G. Karras, M. Ndong, E. Hertz, D. Sugny, F. Billard, B. Lavorel, O. Faucher, Polarization shaping for unidirectional rotational motion of molecules. *Phys. Rev. Lett.* **114**, 103001 (2015).
17. K. Lin, Q. Song, X. Gong, Q. Ji, H. Pan, J. Ding, H. Zeng, J. Wu, Visualizing molecular unidirectional rotation. *Phys. Rev. A* **92**, 013410 (2015).
18. K. Lin, P. Lu, J. Ma, X. Gong, Q. Song, Q. Ji, W. Zhang, H. Zeng, J. Wu, G. Karras, G. Siour, J. M. Hartmann, O. Faucher, E. Gershnabel, Y. Prior, I. S. Averbukh, Echoes in space and time. *Phys. Rev. X* **6**, 041056 (2016).
19. D. Céolin, J.-C. Liu, V. Vaz da Cruz, H. Ågren, L. Journel, R. Guillemin, T. Marchenko, R. K. Kushawaha, M. N. Piancastelli, R. Püttner, M. Simon, F. Gel'mukhanov, Recoil-induced ultrafast molecular rotation probed by dynamical rotational Doppler effect. *Proc. Natl. Acad. Sci. U.S.A.* **116**, 4877–4882, 2019
20. N. B. Simpson, K. Dholakia, L. Allen, M. J. Padgett, Mechanical equivalence of spin and orbital angular momentum of light: An optical spanner. *Opt. Lett.* **22**, 52–54 (1997).
21. Y. Arita, M. Mazilu, K. Dholakia, Laser-induced rotation and cooling of a trapped microgyroscope in vacuum. *Nat. Commun.* **4**, 2374 (2013).
22. S. Kuhn, A. Kosloff, B. A. Stickler, F. Patolsky, K. Hornberger, M. Arndt, J. Millen, Full rotational control of levitated silicon nanorods. *Optica* **4**, 356–360 (2017).
23. R. Reimann, M. Doderer, E. Hebestreit, R. Diehl, M. Frimmer, D. Windey, F. Tebbenjohanns, L. Novotny, GHz rotation of an optically trapped nanoparticle in vacuum. *Phys. Rev. Lett.* **121**, 033602 (2018).
24. J. Ahn, Z. Xu, J. Bang, Y.-H. Deng, T. M. Hoang, Q. Han, R.-M. Ma, T. Li, Optically levitated nanodumbbell torsion balance and GHz nanomechanical rotor. *Phys. Rev. Lett.* **121**, 033603 (2018).
25. J. Ahn, Z. Xu, J. Bang, P. Ju, X. Gao, T. Li, Ultrasensitive torque detection with an optically levitated nanorotor. *Nat. Nanotechnol.* **15**, 89–93 (2020).
26. S. Ospelkaus, K.-K. Ni, G. Quéméner, B. Neyenhuis, D. Wang, M. H. G. Miranda, J. L. Bohn, J. Ye, D. S. Jin, Controlling the hyperfine state of rovibronic ground-state polar molecules. *Phys. Rev. Lett.* **104**, 030402 (2010).
27. J. G. Danzl, M. J. Mark, E. Haller, M. Gustavsson, R. Hart, J. Aldegunde, J. M. Hutson, H.-C. Nägerl, An ultracold high-density sample of rovibronic ground-state molecules in an optical lattice. *Nat. Phys.* **6**, 265 (2010).
28. R. Glöckner, A. Prehn, B. G. U. Englert, G. Rempe, M. Zeppenfeld, Rotational cooling of trapped polyatomic molecules. *Phys. Rev. Lett.* **115**, 233001 (2015).
29. I. S. Vogelius, L. B. Madsen, M. Drewsen, Blackbody-radiation–assisted laser cooling of molecular ions. *Phys. Rev. Lett.* **89**, 173003 (2002).
30. P. F. Staanum, K. Højbjerre, P. S. Skyt, A. K. Hansen, Rotational laser cooling of vibrationally and translationally cold molecular ions. *Nat. Phys.* **6**, 271 (2010).
31. T. Schneider, B. Roth, H. Duncker, I. Ernsting, S. Schiller, All-optical preparation of molecular ions in the rovibrational ground state. *Nat. Phys.* **6**, 275 (2010).
32. R. V. Krems, *Molecules in Electromagnetic Fields: From Ultracold Physics to Controlled Chemistry* (Wiley, 2018).
33. C. P. Koch, M. Lemeshko, D. Sugny, Quantum control of molecular rotation. *Rev. Mod. Phys.* **91**, 035005 (2019).
34. D. Pan, H. Xu, F. J. García de Abajo, Circular dichroism in rotating particles. *Phys. Rev. Lett.* **123**, 066803 (2019).
35. L. M. Zhou, K. W. Xiao, J. Chen, N. Zhao, Optical levitation of nanodiamonds by doughnut beams in vacuum. *Laser Photon. Rev.* **11**, 1600284 (2017).
36. H. Li, Y. Cao, L. M. Zhou, X. Xu, T. Zhu, Y. Shi, C. W. Qiu, W. Ding, Optical pulling forces and their applications. *Adv. Opt. Photonics* **12**, 288–366 (2020).
37. Y. Zheng, L. M. Zhou, Y. Dong, C. W. Qiu, X. D. Chen, G. C. Guo, F. W. Sun, Robust optical-levitation-based metrology of nanoparticle's position and mass. *Phys. Rev. Lett.* **124**, 223603 (2020).
38. T. Zhu, Y. Shi, W. Ding, D. P. Tsai, T. Cao, A. Q. Liu, M. Nieto-Vesperinas, J. J. Sáenz, P. C. Wu, C. W. Qiu, Extraordinary multipole modes and ultra-enhanced optical lateral force by chirality. *Phys. Rev. Lett.* **125**, 043901 (2020).
39. B. A. Garetz, Angular Doppler effect. *J. Opt. Soc. Am.* **71**, 609–611 (1981).
40. P. R. Berman, R. W. Boyd, P. W. Milonni, Polarizability and the optical theorem for a two-level atom with radiative broadening. *Phys. Rev. A* **74**, 053816 (2006).
41. A. Manjavacas, F. J. García de Abajo, Vacuum friction in rotating particles. *Phys. Rev. Lett.* **105**, 113601 (2010).
42. D. Pan, H. Xu, F. J. García de Abajo, Magnetically activated rotational vacuum friction. *Phys. Rev. A* **99**, 062509 (2019).
43. F. Intravaia, M. Oelschläger, D. Reiche, D. A. R. Dalvit, K. Busch, Quantum rolling friction. *Phys. Rev. Lett.* **123**, 120401 (2019).
44. M. S. Rudner, J. C. W. Song, Self-induced Berry flux and spontaneous non-equilibrium magnetism. *Nat. Phys.* **15**, 1017–1021 (2019).
45. A. Asenjo-García, A. Manjavacas, F. J. García de Abajo, Stimulated light emission and inelastic scattering by a classical linear system of rotating particles. *Phys. Rev. Lett.* **106**, 213601 (2011).

Acknowledgments

Funding: This work has been supported, in part, by the European Research Council (ERC Advanced Grant 789104-eNANO), the Spanish MINECO (MAT2017-88492-R and no. SEV2015-0522), the Catalan CERCA Program, Fundació Privada Cellex, and Fundació Mir-Puig. **Author contributions:** D.P. conceived the research and carried out the calculations. D.P. and F.J.G.d.A. developed the theory and wrote the paper. H.X. discussed the results. **Competing interests:** The authors declare that they have no competing interests. **Data and materials availability:** All data needed to evaluate the conclusions in the paper are present in the paper and/or the Supplementary Materials. Additional data related to this paper may be requested from the authors.

Submitted 4 July 2020
Accepted 13 November 2020
Published 6 January 2021
10.1126/sciadv.abd6705

Citation: D. Pan, H. Xu, F. J. García de Abajo, Rotational Doppler cooling and heating. *Sci. Adv.* **7**, eabd6705 (2021).

Rotational Doppler cooling and heating

Deng Pan, Hongxing Xu and F. Javier García de Abajo

Sci Adv **7** (2), eabd6705.
DOI: 10.1126/sciadv.abd6705